

Solar rotation rate and its gradients during cycle 23

H. M. Antia

Tata Institute of Fundamental Research, Homi Bhabha Road, Mumbai 400005, India

antia@tifr.res.in

Sarbani Basu

*Astronomy Department, Yale University, P. O. Box 208101, New Haven CT 06520-8101,
U.S.A.*

basu@astro.yale.edu

and

S. M. Chitre

Centre for Basic Sciences, University of Mumbai, Mumbai 400098, India

kumarchitre@gmail.com

ABSTRACT

Available helioseismic data now span almost the entire solar activity cycle 23 making it possible to study solar-cycle related changes of the solar rotation rate in detail. In this paper we study how the solar rotation rate, in particular, the zonal flows change with time. In addition to the zonal flows that show a well known pattern in the solar convection zone, we also study changes in the radial and latitudinal gradients of the rotation rate, particularly in the shear layer that is present in the immediate sub-surface layers of the Sun. In the case of the zonal-flow pattern, we find that the band indicating fast rotating region close to the equator seems to have bifurcated around 2005. Our investigation of the rotation-rate gradients show that the relative variation in the rotation-rate gradients is about 20% or more of their average values, which is much larger than the relative variation in the rotation rate itself. These results can be used to test predictions of various solar dynamo models.

Subject headings: Sun: oscillations — Sun: rotation — Sun: interior

1. INTRODUCTION

Helioseismology enables us to study dynamics of the solar interior (e.g., Thompson et al. 1996; Schou et al. 1998, etc.). Early results have shown that the differential rotation seen at the solar surface persists till the base of the convection zone and becomes nearly uniform in the radiative interior. Also seen were two shear layers, one near the surface and the other near the base of the convection zone. The latter, which is referred to as the tachocline (Spiegel & Zahn 1992), is generally believed to be the seat of the solar dynamo. Superposed on the relatively smooth latitudinal variation are alternating bands of slightly faster and slower rotation (Kosovichev & Schou 1997).

Data for the last 12 years covering most of the solar cycle 23 are now available from the Global Oscillation Network Group (GONG) project and the Michelson Doppler Imager (MDI) instrument on board SOHO. As a result, it is now possible to study temporal variations of solar dynamics in detail. Early works that used subsets of the data (e.g., Kosovichev & Schou 1997; Schou 1999; Howe et al. 2000a; Antia & Basu 2000) had already established that there is significant variation in the rotation rate of the solar interior. The temporal variation manifests as a system of bands with faster or slower than average rotation rate at fixed depths in the upper layers of the convection zone. And particularly at low latitudes, the zonal flow bands appear to migrate towards the equator with time, and appear to be similar in character to the torsional oscillations discovered in the solar surface rotation rate (Howard & LaBonte 1980; Ulrich et al. 1988; Snodgrass 1992). A subsequent work (Antia & Basu 2001) found that in addition to this pattern at low latitudes, there is another system of zonal-flow bands at high latitudes ($> 45^\circ$) that migrate towards the poles as the solar cycle progresses. With accumulation of more seismic data it has now become clear that these zonal flows penetrate through most of the convection zone (Vorontsov et al. 2002; Basu & Antia 2003, 2006; Howe et al. 2006a). Since the errors in the results obtained by inversions increase with depth, it is not yet clear whether there is any significant temporal variation in the tachocline region near the base of the convection zone — a region where the solar dynamo is believed to be operating. Howe et al. (2000b, 2007) reported a 1.3 year oscillation in the equatorial region around $r = 0.72R_\odot$ during the rising phase of the solar cycle, but that has not been confirmed by other studies (e.g., Antia & Basu 2001; Basu & Antia 2003).

The origin of torsional oscillations or zonal flows is not fully understood, but since the zonal flow banded structure and the magnetic activity pattern seem to be closely related, it is generally believed that zonal flows arise from a nonlinear interaction between magnetic fields and differential rotation. Thus the properties of solar zonal flows should provide a constraint on theories of the solar dynamo. Most dynamo models are kinematic, where the velocity field is specified; such models do not yield any information about temporal variations in

the velocity field. However, there are some non-kinematic dynamo models that include the Lorentz-force feedback on differential rotation, and these have been used to explain the zonal flow patterns. Covas et al. (2000, 2004), for example, considered an axisymmetric mean-field dynamo model to study temporal variations of the rotation rate and of magnetic fields in the solar interior. They found temporal variations in the rotation rate that are qualitatively similar to the zonal-flow pattern inferred from the seismic data. Spruit (2003) suggested that thermal fluctuations due to enhanced emission of radiation by small-scale magnetic fields can drive the zonal-flow pattern. His model produces zonal flows with amplitudes that decrease with increasing depth. Lanza (2007) attempted to find the source of the zonal-flow pattern by using a model for angular momentum transport in the convection zone and by comparing the results with observed patterns. His preliminary results led to constraints on the amplitude, phase and location of the perturbations responsible for the observed torsional oscillations. Rempel (2007) found that the poleward moving branch of zonal flows at high latitude may be explained as a response of the coupled differential rotation/meridional flow system to periodic forcing in mid-latitudes by either Lorentz force or thermal perturbations, with thermal fluctuations very likely playing a role in the low-latitude equator-ward moving branch of the zonal flow.

Most seismic studies hitherto have investigated temporal variations in the rotation rate itself. For the solar dynamo models, however, spatial gradients of this angular velocity are more important. Although the radial gradient of the rotation rate in the outer shear layer has been studied by Schou et al. (1998), Basu & Antia (2001), Corbard & Thompson (2002), etc., a detailed study of the temporal variations of both the radial and latitudinal gradients has not been undertaken so far. This motivated us to further investigate changes in both the radial and the latitudinal gradients of the solar rotation rate with a view to studying temporal variations of the shear pattern. We also study the time-derivative of the rotation velocity, which should relate to the driving forces that are possibly responsible for the zonal flow pattern.

The rest of this paper is organized as follows: we summarize the data and the analysis technique in § 2; our results are described in § 3, and the discussion of our results along with conclusions are given in § 4.

2. Data and technique

We use data obtained by the GONG (Hill et al. 1996) and MDI (Schou 1999) projects in the present work. These data sets consist of the mean frequency and the splitting coefficients for different (n, ℓ) multiplets. Only the odd-order splitting coefficients are required for

determining the rotation rate in the solar interior (e.g., Ritzwoller & Lively 1991). These splitting coefficients are sensitive only to the north-south symmetric component of the rotation rate and hence, that is the only component that can be determined with these data. Consequently, all results shown in this work are symmetric about the equator. There could be an antisymmetric component of rotation present in the Sun, but that cannot be analyzed using the global-mode data used in this work. We use 120 data sets from GONG, each set covering a period of 108 days. The first set starts on 1995, May 7 and the last set ends on 2007, May 15, with a spacing of 36 days between consecutive data sets. Thus there is a considerable overlap between neighboring data sets. The GONG data sets include only p-modes up to $\ell = 150$ and we use all modes with frequencies between 1 and 3.5 mHz. The MDI data sets consist of 56 non-overlapping sets each obtained from observations taken over a period of 72 days. The first set begins on 1996, May 1 and the last set ends on 2007, October 6. Contact with SOHO satellite was lost during June 1998 and the satellite was finally recovered during February 1999. During this period there is only one data set and that covered a period of 60 days. The MDI data sets include f-modes up to $\ell = 300$ and p-modes up to $\ell \approx 200$. We use all modes with frequencies between 1 and 3 mHz. Since the higher frequency modes often cause problems, they have not been included in the analysis. The higher degree modes from MDI are also known to give misleading temporal variations in some cases (e.g., Antia et al. 2003). This is indeed found to be the case for the radial gradient of the rotation rate and is discussed later.

We use a two dimensional Regularized Least Squares (2D RLS) inversion technique as described by Antia et al. (1998) to infer the rotation rate in the solar interior from each of the available data sets. The first 8 odd-order splitting coefficients, a_1, a_3, \dots, a_{15} , were used in the inversions. In order to study the time-variation of the rotation rate we first determine the Sun’s internal rotation rate using each data set, and then take the time average of the results obtained using all data sets at each latitude and depth. Since we treat the GONG and MDI sets separately, we obtain one average result using GONG sets and another using MDI sets. To obtain the time-varying component of rotation, we subtract the mean from the rotation rate at any given epoch. Thus,

$$\delta\Omega(r, \theta, t) = \Omega(r, \theta, t) - \langle \Omega(r, \theta, t) \rangle, \quad (1)$$

where $\Omega(r, \theta, t)$ is the rotation rate as a function of radial distance r , latitude θ and time t . Here the angular brackets denote the average over the time duration for which data are available. As is the case for the time-averaged rotation, the residual rotation rate is calculated separately for GONG and MDI data sets.

For most parts of this investigation we use the residual rotation velocity, $\delta v_\phi = \delta\Omega r \cos \theta$, rather than the rotation rate $\delta\Omega$. This time varying component, δv_ϕ , is generally called

the zonal flow. The definition of zonal flows is somewhat ambiguous: some authors (e.g., Howard & LaBonte 1980) have defined the zonal flows by subtracting the temporal average of a smooth component of the rotation rate. The smooth component is generally defined using three terms (constant, $\sin^2 \theta$ and $\sin^4 \theta$) to calculate the latitudinal variation of rotation rate. There is some difference in the resulting pattern in the two cases, as has been described by Antia & Basu (2000). In this work we adopt the definition given by Eq. (1) where the temporal mean of the full rotation rate is subtracted to obtain the residuals. This definition has been used previously by other investigators too (e.g., Howe et al. 2000a, 2005, 2006a; Antia & Basu 2001; Basu & Antia 2003, 2006, etc.).

For the purpose of investigating the spatial gradients of the rotation rate, we use Ω rather than v_ϕ and calculate the radial gradient, ($\Omega_{,r} \equiv \partial\Omega/\partial r$), as well as the latitudinal gradient ($\Omega_{,\theta} \equiv (1/r)\partial\Omega/\partial|\theta|$). These derivatives are computed numerically. Since the inferred zonal flow pattern is symmetric about the equator, the radial gradient is also symmetric. The latitudinal gradient on the other hand is antisymmetric about the equator, and hence it is 0 at the equator. To restore the symmetry of the latitudinal gradient we, have defined the gradient with respect to the absolute value of the latitude. With this definition, both $\Omega_{,r}$ and $\Omega_{,\theta}$ are symmetric about the equator. Since the 2D RLS technique used for inversion gives results that are smooth in (r, θ) , there is no difficulty in computing these derivatives numerically. The errors in these derivatives are, of course, larger than those in Ω itself. The time-varying component of these derivatives is calculated by differentiating the residual in rotation rate defined by Eq. (1), i.e., $\delta\Omega_{,r} \equiv \partial\delta\Omega/\partial r$ and $\delta\Omega_{,\theta} \equiv (1/r)\partial\delta\Omega/\partial|\theta|$.

We also calculate the derivative of the rotation velocity v_ϕ with respect to time (note that $\partial v_\phi/\partial t = \partial\delta v_\phi/\partial t$), since it is likely to give an indication of the forcing term that drives the zonal-flow pattern. For calculating time-derivatives numerically, we need v_ϕ at different times, which we obtain from independent data sets. It should be noted that since the magnitude of the zonal-flow velocity is small, the temporal derivative has significant errors. To get more reliable estimates, we smooth δv_ϕ at each latitude and radius by assuming that the temporal variation is periodic with a period of 11 years. Since the variation is not strictly sinusoidal, we also include a few higher harmonics and fit the following functional form to δv_ϕ :

$$\delta v_\phi(r, \theta, t) = \sum_{k=1}^{k_{\max}} a_k(r, \theta) \sin(k\omega_0 t) + b_k(r, \theta) \cos(k\omega_0 t) = \sum_{k=1}^{k_{\max}} A_k \sin(k\omega_0 t + \phi_k) . \quad (2)$$

In the above equation, ω_0 is the basic frequency for the fundamental component, which is assumed to have a period of 11 years. The coefficients a_k and b_k are determined by a least squares fit at fixed values of (r, θ) . These coefficients determine the amplitude, A_k and phase, ϕ_k of the variation at any point defined by the values of (r, θ) for each harmonic of the 11

year period. We choose time $t = 0$ to be the beginning of GONG data sets and the phase is measured with respect to that epoch. This zero-point is about a year before the minimum phase of solar activity. Three terms are found to be sufficient to fit the data. Similar fits were also used by Vorontsov et al. (2002), Basu & Antia (2003, 2006) and Howe et al. (2005, 2006a). These fits are then used to calculate the time-derivative. These fits also enable us to extend the pattern beyond the epochs for which observations exist. These extended patterns are often useful in comparing the observed pattern with those obtained on the basis of dynamo models since dynamo-model predictions are traditionally shown over a period of 22 years.

3. RESULTS

The rotation rate in the solar convection zone exhibits temporal variations. Near the solar surface the pattern is observed to be similar to the well known torsional oscillations detected at the surface. In what follows we describe our results in detail. We include results on the temporal variation as well as results on the radial, latitudinal and time derivatives of the rotation rate.

Before discussing temporal variations we examine the time-averaged quantities. Since the mean rotation rate inferred by the inversion of seismic data is well-known (e.g., Thompson et al. 1996; Schou et al. 1998), we do not show the results here, but instead we only show the results for the gradients, $\Omega_{,r}$ and $\Omega_{,\theta}$. The upper panels of Fig. 1 show the cuts at fixed latitude, while the lower panels show the color-coded results as a function of both r and θ .

The radial gradient of the solar rotation rate is large in the outer shear layer as well as in the tachocline, and is small in other regions. Below the outer shear layer, the radial gradient is positive in the low latitude regions, and is negative in all other regions wherever it can be determined reliably. In the outer shear layer, we find an average negative gradient of the order of a few 100 nHz R_{\odot}^{-1} i.e, $10^{-15} \text{ m}^{-1} \text{ s}^{-1}$. The value of $\Omega_{,r}$ is largely independent of latitude in the outer shear layer, except perhaps at very high latitudes. It should be noted that the regularization used in carrying out the inversions smooths out the radial variations near the tachocline region and hence the actual radial gradient in the tachocline region is expected to be much larger. If the tachocline model obtained by Antia et al. (1998) is used to define the rotation rate in the tachocline region, the gradient can be calculated more precisely, and the results obtained using MDI data are shown in Fig. 2. It is clear that the gradient is much larger and more localized in the tachocline region than is seen in Fig. 1. The exact shape of the curves, of course, depend on the tachocline model used and may not have much significance. The gradient in the latitudinal direction is significant only

within the convection zone, this is of course expected since this is where we find differential rotation. The maximum value of the latitudinal gradient is comparable to the radial gradient in the outer shear layer. This gradient is negative almost everywhere. When studying the temporal evolution of the two gradients, we compare the magnitude of the time-variation with the corresponding time-averaged values.

Although the pattern of variation of these gradients is similar for results obtained with GONG and MDI data, the actual values show significant differences in some regions. The results obtained from the two data sets agree reasonably well as far as the latitudinal gradient is concerned, though there are differences at high latitudes. There are noticeable differences in the radial gradients obtained from the two data sets, particularly in the outer shear layer. Such differences between results from GONG and MDI data have been seen even for the rotation rate itself (e.g., Schou et al. 2002), and the reasons for this disagreement are not fully understood. This issue is discussed further in connection with the temporal variations of the radial gradient.

3.1. The time-variation of the rotational velocity: the zonal flows

Fig. 3 shows the residual rotational velocity $\delta v_\phi = \delta\Omega r \cos\theta$ obtained using GONG data. Results are shown at a few representative radii in the convection zone. The figure shows the expected, distinct, bands of faster and slower-than-average rotation velocity that, at low latitudes, move towards the equator with time. At high latitudes, the bands seem to move towards the poles. The slow band at high latitudes reaches its end near the poles around 2001, the time when the polar field reversed, while the fast band at high latitude, on the other hand, appears to terminate around 1996 (and will probably do so again in 2008) near the minimum of solar activity. The transition between the equator-ward and pole-ward movements takes place at a latitude of around 45° . At high latitudes it appears that the 12 years of GONG data have covered a little more than one period, but at low latitudes the periodicity of the zonal-flow pattern is not obvious. The zonal-flow pattern in the outer shear layer appears to be more complex at low latitudes than at high latitudes. In this layer, the low-latitude fast-moving bands from the two hemispheres appear to have merged around 2000, but seem to split around 2005, and then merge again in 2007. A band of fast rotation appears near a latitude of 35° in both hemispheres around 2005 and we believe that these bands are a precursor to the next solar cycle. In fact, a closer examination of the figure suggests that these bands have a weak connection to the bands that started at 50° latitude around 1997 and then bifurcated around 2004 into one branch that moved polewards and another that moved towards the equator. These bands should reach the equator and merge

during the next maximum phase of solar activity. Thus the band which started near the 50° latitude zone in 1997, i.e., just after the minimum phase of the activity, is expected to reach the equator during the maximum of the following cycle, and will thus span a period of 15–18 years. The band of slow rotation that started a few years after the last solar-activity maximum around a latitude of 50° would reach the equator some time after the next minimum, again spanning a period of about one and a half times the fiducial solar cycle.

Figure 3 also shows the zonal flow-pattern obtained using GONG data as cuts at a few representative latitudes. These can be used to determine how the zonal-flow pattern changes with radial distance. At low latitudes there is a clear trend of the pattern moving upwards with time and it is also clear that the pattern penetrates through most of the convection zone, probably reaching down to the base of the convection zone. At these low latitudes the average rate of upward movement appears to be about $0.05R_\odot$ per year or about 1 m s^{-1} . This follows from the fact that Fig. 3 shows the band moving from close to the base of the convection zone to surface in about 6 years. At a latitude of 60° too the band of faster rotation appears to penetrate nearly to the base of the convection zone near the maximum of solar activity.

The changing pattern of the zonal flows implies that the maximum and minimum velocities of the flow occur at different times for different latitudes and depths. This has also been found by Schou (1999) and Howe et al. (2000a). Fig. 4 shows the zonal-flow velocity, δv_ϕ , at different latitudes as a function of time at $r = 0.98R_\odot$. Both GONG and MDI results are shown and as can be seen, there is good agreement between the results obtained using data from the two projects. It is clear that the time-dependence of δv_ϕ changes with latitude. While the high latitudes show a nearly sinusoidal variation with a possible period of close to 11 years, the variation at low latitudes is more complicated. The Fourier transform of the results at all latitudes show a peak at the lowest frequency bin, which corresponds to a period of about 11 years. The pattern at low latitudes, however, is clearly not sinusoidal. Thus if it is periodic, higher harmonics must be present. Vorontsov et al. (2002) and Basu & Antia (2003) had found the third harmonic to be important. But those studies were based on data covering only about half the solar cycle. With more data Howe et al. (2005) and Basu & Antia (2006) found the second harmonic to be more significant than the third harmonic. Clearly data from cycle 24 will be needed to establish the periodicity properly. At a latitude of around 50° , the amplitude of the flows is distinctly smaller than that at other latitudes. This is close to the latitude where the switch from the equator-ward movement to pole-ward movement of the flows occurs. Thus regions around this latitude seem to separate the two branches of the zonal-flow pattern.

While it is not possible to confirm the periodicity of the flows with current data sets, it is tempting to assume a period comparable to the average solar cycle. Thus we assume that the pattern is periodic with a period of 11 years and fit it using Eq. (2) with 3 terms. The amplitudes of the first two terms are shown in Fig. 5 for results obtained from both GONG and MDI data. Both these data sets give similar results and it is clear that although the amplitude of the dominant $k = 1$ component decreases with depth, the pattern appears to penetrate to the base of the convection zone. The highest amplitude, of up to 10 m s^{-1} , is seen in the outer $0.1R_{\odot}$ at high latitudes. The amplitude is small in the mid-latitude region around 45° . It is clear that the $k = 2$ harmonic is significant, however, its magnitude is much smaller than that for the first term. The amplitude of the third term is found to be even smaller and it is difficult to estimate the amplitude reliably. The relative magnitude of the various harmonics may depend on the origin of the zonal flow pattern. In the very deep layers close to the tachocline, the errors in the zonal-flow velocity estimates are so large that it is difficult to assign any significance to the fluctuating results obtained there. Below the convection zone the amplitude of both harmonics is very small, indicating that solar cycle-related variations are not clearly seen in these layers.

Fig. 5 also shows the phase of the $k = 1$ term obtained from both GONG and MDI data. It is clear that at low latitudes the phase changes rather steeply around $r = 0.9R_{\odot}$. At high latitudes while MDI results show very little phase variation with depth, GONG results do show some variations. It is not clear if these differences are significant. In the outer half of the convection zone, both GONG and MDI results appear to show a sharp transition around a latitude of 40° . This may mark the transition between the low and high latitude patterns. There is good agreement between the GONG and MDI results.

We can extend the zonal flow pattern over longer time intervals if we assume that the fitted parameters do not change from cycle to cycle, and the resulting pattern can be compared with predictions from different dynamo models. We shall be happy to make such figures available for investigators who wish to make use of them.

3.2. Temporal variations of the rotation-rate gradients

We calculated the time variation of both radial and latitudinal gradients by numerical differentiation of the rotation-rate residuals that were obtained using Eq. (1). Figures 6 and 7 show the two components of the gradient at different latitudes as a function of time at $r = 0.95R_{\odot}$. There is a reasonable agreement between results obtained using GONG and MDI data at this depth. It is clear that there is significant time-variation in these gradients and that the amplitude of the variation is a sizable fraction of its average value. At low

latitudes, the temporal variation of the radial gradient turns out to be about 20% of its average value. The relative variation in the latitudinal gradient is similar. These changes are much larger than the temporal variation in the rotation rate, which is only about 0.1–1% of its average value. As a result, we expect this time-variation in the angular velocity gradients to play an important role in workings of the solar dynamo.

In order to establish a possible relation between the zonal-flow bands and the magnetic cycle, we compare the pattern of temporal variations of $\delta\Omega_{,r}$ and $\delta\Omega_{,\theta}$ at $r = 0.95R_{\odot}$ with the butterfly diagram seen in the distribution of sunspots. The results are shown in Fig. 8. We have chosen this depth because GONG and MDI results for the radial gradient do not agree well in shallower layers. We have multiplied the gradients by $\cos\theta$ in this and subsequent figures in order to compensate for the increase in $\delta\Omega$ with latitude. This factor is already present in the residual rotation velocity δv_{ϕ} since it is part of the conversion from Ω to v_{ϕ} . As a result of this factor residuals in v_{ϕ} show little variation in amplitude with latitude, and with this factor, residuals in $\delta\Omega_{,r}$ or $\delta\Omega_{,\theta}$ also show a similar behavior. It can be seen from Fig. 8 that the sunspots are mainly concentrated in regions where the radial gradient is larger than its average value and where the latitudinal gradient is smaller than the average gradient. Note, the mean values of both these gradients are negative at this depth, and hence their magnitude will be larger in regions where $\delta\Omega_{,r}$ or $\delta\Omega_{,\theta}$ are negative. Thus the sunspots are found to occur in regions where the magnitude of radial gradient is smaller than average and that of the latitudinal gradient is larger than average. Clearly, the butterfly pattern is related to zonal flows, as was, indeed, noted earlier by Snodgrass (1987). Around 2005, when the equatorial zonal flow band of faster rotation splits, the latitudinal gradient of rotation rate flips sign in low latitude region.

The errors in our results on the gradients are naturally expected to be larger than those in $\delta\Omega$. These large errors give rise to some of the fluctuations seen in Figs 6 and 7. As in the case of δv_{ϕ} , these fluctuations can be smoothed by fitting a periodic signal with a period of 11 years to the results using Eq. (2). The fitted results, extended to a period of 22 years, are shown in Figs. 9,10. The pattern of bands of higher and lower than average gradients can be seen in these figures too, with low latitude bands moving towards the equator and the pattern once again changing at high latitudes. In general there is reasonable agreement between GONG and MDI results, except in the case of the radial gradient at $r = 0.98R_{\odot}$ where there are significant differences between the two results. The agreement between GONG and MDI results is better in deeper layers, despite the fact that the gradient itself is much smaller. As far as the latitudinal gradient is concerned, the agreement between GONG and MDI results is good at all depths. It has been known for some time that there are differences between GONG and MDI rotational-splitting data (Schou et al. 2002). These differences result in the differences between results obtained with GONG and MDI

data about the outermost layers at all latitudes. The most prominent difference is however, in the radial-gradient of the rotation rate at high latitudes. MDI data shows the presence of a jet like feature at high latitudes while GONG data do not (e.g., Howe et al. 1998, Schou et al. 2002). Interestingly, the differences between the GONG and MDI data do not affect the time variations of the zonal-flow velocities and the results obtained from the two different data sets agree reasonably well. This may indicate that the systematic differences between the two data sets are largely independent of time. Since we calculate the residual $\delta\Omega$ independently for GONG and MDI the systematic errors cancel when the mean value is subtracted in Eq. (1).

It is tempting to speculate that the difference in radial gradient in outer layers between the MDI and GONG results is because of the presence of higher degree modes, in particular the f-modes, in MDI data sets. To test this, we repeated the calculations by removing these modes and find that the results remain largely unaffected. Thus the difference between GONG and MDI results is unlikely to be due to difference in resolution due to presence of extra modes and possibly represents the difference in splitting coefficients themselves as found by Schou et al. (2002). While the zonal velocity, δv_ϕ , computed using the two data sets agree reasonably well, the time variation of the radial gradient of the inversions show significant differences. Thus the process of determining the radial gradient and its time variation appears to amplify the differences. In order to identify the modes that lead to this difference, we did one more set of inversions for MDI data using only modes with $\ell < 120$; the resulting radial gradient is closer to the result obtained using GONG data as can be seen from Fig. 11. Thus it is clear that the differences are caused by the high-degree modes in the MDI sets. Similar problems have been noticed in even-order splitting coefficients from MDI (Antia et al. 2003). A closer look at Fig. 9 suggests that at $r = 0.98R_\odot$ there was a rather sharp change around 1999 which is around the period when contact with SOHO was re-established. This is similar to the results on asphericity found by Antia et al. (2003) and results on solar radius variations found by Antia (2003). All these could be due to some systematic error introduced during recovery of SOHO. High-degree modes which are trapped in the outer layers do not seriously affect the inversion results in the deeper layers and hence, these layers are not affected by the possible problems with the MDI high-degree modes. The re-analysis of MDI data has shown that there are some removable problems with the currently available data sets (Larson & Schou 2007).

The pattern at high latitudes is complicated and it is not possible to say with any certainty whether the pattern is moving towards the poles or towards the equator. From Fig. 9 it can be seen that at $r = 0.95R_\odot$, the band with lower than average radial gradient that started around a latitude of 50° in about 1995 ends at the equator around 2012, thus spanning a period of about one and a half fiducial solar cycles. This is similar to the corresponding

band in the zonal-flow pattern. However, unlike the bands in the zonal-flow pattern, these bands appear to last for only about a solar cycle in the latitudinal-gradient pattern. From the panels in Fig. 9 that show the radial dependence of $\Omega_{,r}$ it also appears that the pattern rises upwards with time at low latitudes. At the latitude of 30° the amplitude of the variation in the radial gradient is rather small. This is the latitude where the radial gradient in the lower convection zone changes sign (cf., Fig. 1) and the magnitude of temporally averaged $\Omega_{,r}$ is small too. At high latitudes ($> 45^\circ$) the bands showing the changes in the radial gradient penetrate to the base of the convection zone, while at low latitudes the amplitude decreases below the outer shear layer and there is a distinct phase shift around $r = 0.9R_\odot$. For the latitudinal gradient, the temporal variations are generally significant only in the outer shear layer and below a depth of $0.1R_\odot$ this component is generally small (Fig. 10).

3.3. The time derivative of v_ϕ

We evaluate the time-derivative of δv_ϕ , the zonal-flow velocity, by differentiating the fits in Eq. (2). The results are shown in Fig. 12. As expected, the magnitude of the derivative is of the order of $\omega_0|\delta v_\phi|$, i.e., about 10^{-7} m s $^{-2}$. Since this derivative is calculated by differentiating Eq. (2), the pattern of the derivative is essentially similar to that of δv_ϕ , except for a phase shift of $\pi/2$. However, the higher harmonics make a larger contribution to the zonal-flow derivative than to the flow itself and as a result, there are additional differences between the patterns that can be seen when the pattern of the zonal-flow derivative is compared to the pattern of the zonal flow. The second and third harmonics appear to dominate in the deeper parts of the convection zone near the tachocline, but since the signal in this region is fairly weak even in δv_ϕ , it is not clear if this is significant.

4. DISCUSSION AND CONCLUSIONS

We have studied the time-variation of the solar-internal rotation rate and its gradients over almost the entire period covering solar cycle 23 using data from the GONG and MDI projects. We used the rotation-rate residuals obtained by subtracting the time-averaged rotation rate from that at each epoch at a given latitude and depth to study the zonal-flow pattern and to determine how it changes with time. These residuals have also been used to study the radial and latitudinal gradients of the zonal flows as well as the time-derivative of solar rotation velocity. Our main results are as follows:

1. The rotation-velocity residuals show the well known pattern similar to the observed

pattern of torsional oscillations at the solar surface. At low latitudes the results show bands of faster and slower-than-average rotation speed moving towards the equator as the solar cycle progresses. At high latitudes on the other hand, these bands move towards the poles. The transition between the equator-ward and pole-ward movement occurs around a latitude of 45° .

2. We find a precursor of the next solar cycle in the form of a band of fast rotation that appeared at about the 35° latitude near the surface around 2005 when the Sun was approaching the activity minimum. We also find that the band of faster rotation found in the region near the equator appears to have bifurcated around the same time.
3. The zonal flow pattern at low latitudes moves upwards, towards shallower depths, with an average speed of about 1 m/s.
4. The relative time variation of the radial gradient of the rotation-rate is about 20% of its average value, which is much larger than the relative variation in the rotation rate itself. The time variation of the latitudinal gradient is large only in the outer $0.1R_\odot$ of the Sun, the maximum change being about 20% of the mean value.
5. The magnetic butterfly diagram coincides with band of larger than average radial gradient and with smaller than average latitudinal gradient at $r = 0.95R_\odot$. Noting that both gradients are negative, the sunspot activity bands occurs in regions of enhanced latitudinal shear and diminished radial shear, as compared to the magnitude of the average shear.
6. The time derivative of the rotation velocity is about 10^{-7} m s^{-2}

The equator-ward movement of the zonal-flow pattern at low latitudes is well known (Schou 1999; Howe et al. 2000a; Antia & Basu 2000; Vorontsov et al. 2002). The pole-ward migrating high latitude branch has also been noted earlier by Antia & Basu (2001) and Ulrich (2001). The transition between the equator-ward and pole-ward movements occurs around a latitude of 45° . The differences between the low-latitude and the high-latitude pattern also manifests in integrated quantities like the rotational kinetic energy and angular momentum (Antia et al. 2008). The time-variations of the rotational kinetic energy integrated separately over low and high latitude regions also differ. The high-latitude regions show a kinetic-energy variation that is correlated with the solar activity throughout the convection zone. At the low latitudes, on the other hand, the positive correlation between kinetic energy and solar activity exists only in the outer $0.1R_\odot$, while the variations are anticorrelated with solar activity in the rest of the convection zone. Observations of magnetic features at the solar surface also show an equator-ward movement at low latitudes (manifesting in the well-known butterfly

diagram) and a pole-ward movement at high latitudes (e.g., Leroy & Noens 1983; Makarov & Sivaraman 1989; Erofeev & Erofeeva 2000; Benevolenskaya et al. 2001). Theoretical models of the solar dynamo, such as those of Covas et al. (2000, 2001), Bushby (2005) show these features, though they do differ in detail, such as in the phase. The predicted butterfly diagrams of many models (Jiang et al. 2007; Rempel 2006, etc.) also show a low-latitude equator-ward moving branch and a high-latitude pole-ward drifting branch.

The splitting of the band marking fast rotating region near the equator appears to be a new feature and we are not aware of any other investigations that have noted this. Although we have shown only GONG results, MDI data also show the splitting of the bands. The observations during the last solar minimum, however, does not show this feature clearly. Although, a closer look at the Fig. 3 shows a faint signature of two bands merging at the equator around 1996, albeit with a magnitude of δv_ϕ around 0.5 m s^{-1} , which is comparable to the error estimates and about a factor of 5 lower than the corresponding value around 2006. This difference could indeed be owing to cycle to cycle variation. We clearly need more data to see the development of this pattern. The near-surface behavior of zonal flows can be seen in the surface rotation rate data from Mt. Wilson (Ulrich 2001; Howe et al. 2006b) that also covers the previous solar cycle. Since the errors in these observations are larger, it is difficult to say whether the splitting of the near equator band was seen in these results during the last cycle.

The rise of the zonal flow pattern with time has been seen in sub-surface layers from other measurements too. Conclusions similar to ours were drawn by Komm, Howard & Harvey (1993) who compared the zonal flow pattern obtained using the Doppler measurements at the surface with that from magnetic features that are believed to be anchored underneath the surface. Our result that the zonal flows penetrate through a good fraction of the convection zone, and probably reach the base of the convection zone appears to contradict early inferences (Howe et al. 2000a; Antia & Basu 2000) that these flows penetrate only to a radius of $0.9R_\odot$. The early results could have been due to the fact that the phase of the zonal flow pattern at low latitudes changes around this depth. With limited data this could have lead to the conclusion that the pattern does not penetrate below this depth. This phase change is seen in variation of rotational kinetic energy in low latitudes too (Antia et al. 2008). Our results are, however, similar to those of Vorontsov et al. (2002), Basu & Antia (2003) and Howe et al. (2005). Vorontsov et al. (2002) also found that a band of faster rotating elements appears to penetrate almost up to the base of the convection zone at latitude of around 60° . Dynamo models that assume that the tachocline is the seat of the dynamo (e.g., Covas et al. 2000, 2001, 2004; Bushby 2005, etc.) also predict that the zonal flow pattern should persist through the convection zone.

The possible link between time-dependent shear oscillation pattern and the solar activity cycle was first emphasized by Snodgrass (1987). This becomes evident from a striking resemblance of shear zones with the magnetic activity bands revealed through the butterfly diagram (Fig. 8). Making the assumption that seat of the solar dynamo is likely to be located within the shear layers, the observational information that we have gained from the time-variation of radial and latitudinal gradients of rotation rate should provide a valuable input for understanding the dynamo mechanism.

We have hitherto been concerned largely with the time-variations of the global rotation rate which is about 0.1–1% of its mean value. The relative temporal variations in the radial and latitudinal gradients of the rotation rate, however, turn out to be larger, 20% or more of their mean values. Clearly, the time-varying shear pattern in the activity bands must play an important role in driving the magnetic cycle. In fact, the time-derivatives of angular velocity may be used either as valuable input for dynamo models or at any rate as a constraint on them. Indeed, the time derivative of the differential rotation has been effectively used in dynamo models such as those of Covas et al. (2000) and Rempel (2006).

It is illustrative to consider the azimuthal components of the induction and momentum equations and neglect the presence of other velocity field such as meridional circulation and dissipation, and write the equations

$$\frac{\partial B_\phi}{\partial t} = r \cos \theta \mathbf{B}_p \cdot \nabla \Omega, \quad (3)$$

$$\rho \frac{\partial v_\phi}{\partial t} = \frac{1}{4\pi r \cos \theta} \nabla \cdot (\mathbf{B}_p (r \cos \theta B_\phi)), \quad (4)$$

where \mathbf{B}_p and B_ϕ are respectively the poloidal and toroidal components of the magnetic field, and ρ is the density which is assumed to be independent of time (e.g., Basu & Antia 2000; Basu 2002). With the available knowledge of the time-dependent radial and latitudinal gradients of the angular velocity, it should be feasible to deduce the temporal variation of the toroidal magnetic field for an assumed configuration of the poloidal field. Equally, the force term can also be estimated using the measured acceleration $\partial v_\phi / \partial t$ provided we assume that the solar torsional oscillations are driven mainly by the Lorentz force, although there will be additional contributions from the temporally varying meridional flow (e.g., Haber et al. 2002; Basu & Antia 2003) which we neglect. To an order of magnitude we can write

$$\frac{\partial v_\phi}{\partial t} \approx \frac{|\mathbf{B}_p| B_\phi}{4\pi r \rho}, \quad (5)$$

If the magnitude of the poloidal field is estimated through independent means, it should be possible to infer the strength of the azimuthal field using our knowledge of $\partial v_\phi / \partial t$. Thus, if the magnitude of both poloidal and toroidal components are comparable, then the magnetic

field would be of the order of 1 G near the surface increasing to 1000 G near the base of the convection zone. The surface value is consistent with observations of the average magnetic field at the surface (e.g., Ulrich & Boyden 2005). Since the magnetic field is generally concentrated in flux tubes with low filling factors, the magnetic field in these flux tubes is expected to be much higher. On the other hand, if the poloidal field is 100 times weaker than the toroidal field (e.g., Rempel 2007) then the toroidal field will be about 10 times the above estimate, i.e., of the order of 10 kG near the base of the convection zone.

In conclusion, we emphasize that observations of the zonal flows of the Sun now cover almost an entire solar cycle, and there are some features of the flows seen at this solar minimum phase that had not been noticed in the earlier solar minimum for which the helioseismic data were sparse. The further evolution of these features should shed light on the differences between different solar cycles. The current results are also precise enough to provide important inputs to or constraints for solar dynamo models.

This work utilizes data obtained by the Global Oscillation Network Group (GONG) project, managed by the National Solar Observatory, which is operated by AURA, Inc. under a cooperative agreement with the National Science Foundation. The data were acquired by instruments operated by the Big Bear Solar Observatory, High Altitude Observatory, Learmonth Solar Observatory, Udaipur Solar Observatory, Instituto de Astrofísica de Canarias, and Cerro Tololo Inter-American Observatory. This work also utilizes data from the Solar Oscillations Investigation/ Michelson Doppler Imager (SOI/MDI) on the Solar and Heliospheric Observatory (SOHO). SOHO is a project of international cooperation between ESA and NASA. MDI is supported by NASA grants NAG5-8878 and NAG5-10483 to Stanford University. SB acknowledges partial support from NSF grant ATM 0348837. SMC thanks the Indian National Science Academy for support under the INSA Honorary Scientist programme.

REFERENCES

- Antia, H. M. 2003, *ApJ*, 590, 567
- Antia, H. M., & Basu, S. 2000, *ApJ*, 541, 442
- Antia, H. M., & Basu, S. 2001, *ApJ*, 559, L67
- Antia, H. M., Basu, S., & Chitre, S. M. 1998, *MNRAS*, 298, 543
- Antia, H. M., Chitre, S. M., Gough, D. O. 2008, *A&A*, 477, 657

- Antia, H. M., Chitre, S. M., Thompson, M. J. 2003, *A&A*, 399, 329
- Basu, S. 2000, in proc. SOHO 11, From Solar Min to Max: Half a Solar Cycle with SOHO, ed., A. Wilson, ESA SP-508 p. 7
- Basu, S., & Antia, H. M. 2000, *Sol. Phys.*, 192, 449
- Basu, S., & Antia, H. M. 2001, in Proc. SOHO 10/GONG 2000 Workshop: Helio- and asteroseismology at the dawn of the millennium, Eds., A. Wilson, P. L. Pallé, ESA SP-464, p. 179
- Basu, S., & Antia, H. M. 2003, *ApJ*, 585, 553
- Basu, S., & Antia, H. M. 2006, in proc. SOHO 18/GONG 2006/HELAS I, Beyond the spherical Sun (ESA SP-624) eds., K. Fletcher, M. J. Thompson, p. 128
- Benevolenskaya, E. E., Kosovichev, A. G., & Scherrer, P. H. 2001, *ApJ*, 554, L107
- Bushby, P. J. 2005, *AN*, 326, 218
- Corbard, T., & Thompson, M. J. 2002, *Solar Phys.*, 205, 211
- Covas, E., Tavakol, R., Moss, D., & Tworkowski, A. 2000, *A&A*, 360, L21
- Covas, E., Tavakol, R., & Moss, D. 2001, *A&A*, 371, 718
- Covas, E., Moss, D., & Tavakol, R. 2004, *A&A*, 416, 775
- Erofeev, D. V., & Erofeeva, A. V. 2000, *Sol. Phys.*, 191, 281
- Haber, D. A., Hindman, B. W., Toomre, J., Bogart, R. S., Larsen, R. M., Hill, F. 2002, *ApJ*, 570, 855
- Hill, F., et al. 1996, *Sci.*, 272, 1292
- Howard, R., & LaBonte, B. J. 1980, *ApJ*, 239, L33
- Howe, R., Antia, H., Basu, S., Christensen-Dalsgaard, J., Korzennik, S. G., Schou, J. & Thompson, M. J. 1998, in Proc. SOHO6/GONG98, “Structure and Dynamics of the Interior of the Sun and Sun-like Stars,” eds. S. Korzennik, A. Wilson, ESA SP 418, 803
- Howe, R., Christensen-Dalsgaard, J., Hill, F., Komm, R. W., Larsen, R. M., Schou, J., Thompson, M. J., & Toomre, J. 2000a, *ApJ*, 533, L163

- Howe, R., Christensen-Dalsgaard, J., Hill, F., Komm, R. W., Larsen, R. M., Schou, J., Thompson, M. J., & Toomre, J. 2000b, *Sci*, 287, 2456
- Howe, R., Christensen-Dalsgaard, J., Hill, F., Komm, R. W., Schou, J., Thompson, M. J. 2005, *ApJ*, 634, 1405
- Howe, R., Rempel, M., Christensen-Dalsgaard, J., Hill, F., Komm, R. W., Larsen, R. M., Schou, J., Thompson, M. J. 2006a, *ApJ*, 649, 1155
- Howe, R., Komm, R. W., Hill, F., Ulrich, R., Haber, D. A., Hindman, B. W., Schou, J., Thompson, M. J. 2006b, *Solar Phys.*, 235, 1
- Howe, R., Christensen-Dalsgaard, J., Hill, F., Komm, R. W., Schou, J., Thompson, M. J., Toomre, J. 2007, *Adv. Space Res.*, 40, 915
- Jiang, J., Chatterjee, P., & Choudhury, A. R. 2007, *MNRAS*, 381, 1527
- Komm, R. W., Howard, R. F., & Harvey, J. W. 1993, *Sol. Phys.*, 143, 19
- Kosovichev, A. G., & Schou, J. 1997, *ApJ*, 482, L207
- Lanza, A. F. 2007, *A&A*, 471, 1011
- Larson. T., Schou, J. 2007, in *Proc. Helioseismology, Asteroseismology and MHD Connections*, *J. Phys. Conf. Ser.*, in press
- Leroy, J. -L., & Noens, J. -C. 1983, *A&A*, 120, L1
- Makarov, V. I., & Sivaraman, K. R. 1989, *Sol. Phys.*, 123, 367
- Rempel, M. 2006, *ApJ*, 647, 662
- Rempel, M. 2007, *ApJ*, 655, 651
- Ritzwoller, M. H., & Lavelly, E. M. 1991, *ApJ*, 369, 557
- Schou, J. 1999, *ApJ*, 523, L181
- Schou, J., et al. 1998, *ApJ*, 505, 390
- Schou, J., et al. 2002, *ApJ*, 567, 1234
- Snodgrass, H. B. 1987, *Solar Phys.*, 110, 35
- Snodgrass, H. B. 1992, in *The Solar Cycle*, *Proc. NSO 12th Summer Workshop*, ed., K. L. Harvey, *ASPS* 27, 205

- Spiegel, E. A., & Zahn, J.-P. 1992, *A&A*, 265, 106
- Spruit, H. C. 2003, *Solar Phys.*, 213, 1
- Thompson, M. J., et al. 1996, *Sci.*, 272, 1300
- Ulrich, R. K. 2001, *ApJ*, 560, 466
- Ulrich, R. K. & Boyden, J. E. 2005, *ApJ*, 620, L123
- Ulrich, R. K., Boyden, J. E., Webster, L., Snodgrass, H. B., Padilla, S. P., Gilman, P., & Shieber, T. 1988, *Sol. Phys.*, 117, 291
- Vorontsov, S. V., Christensen-Dalsgaard, J., Schou, J., Strakhov, V. N., & Thompson, M. J. 2002, *Sci.*, 296, 101

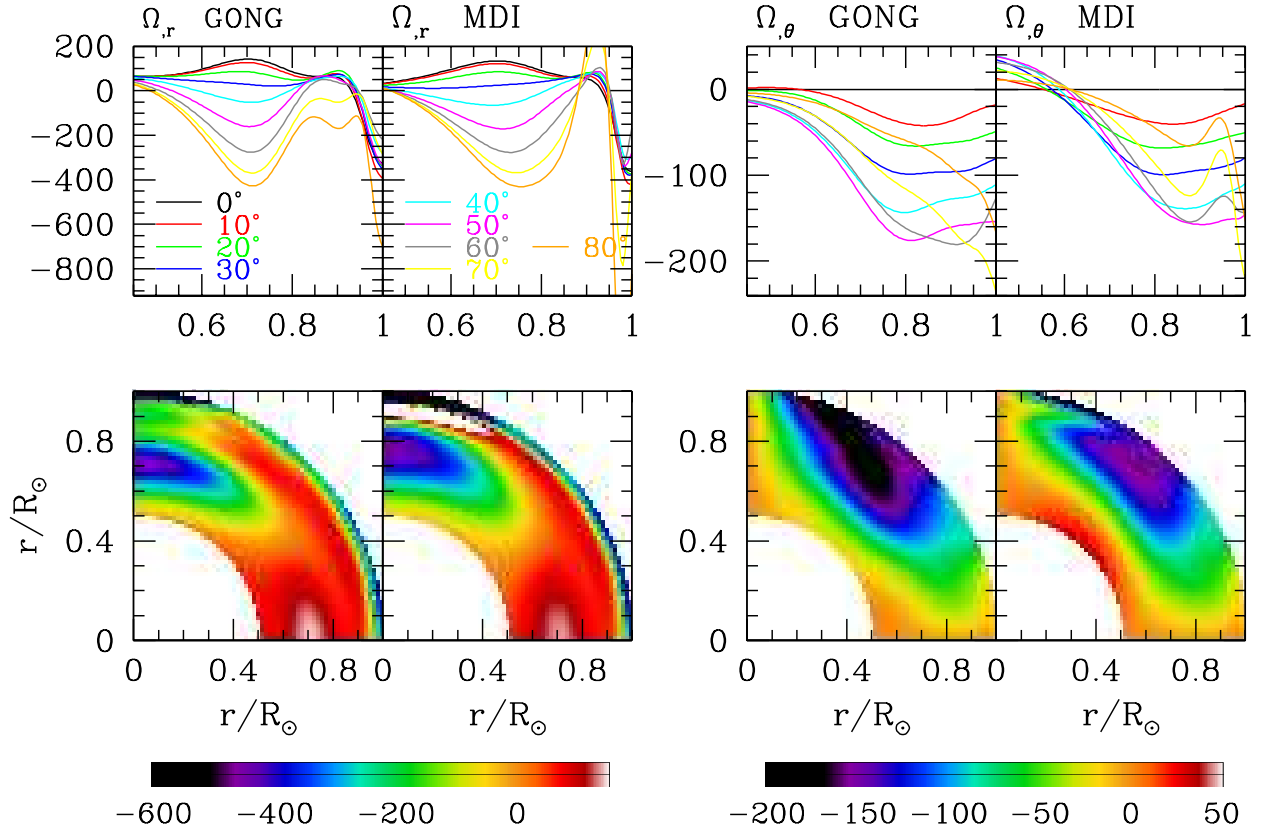


Fig. 1.— The mean radial gradient, $\Omega_{,r}$, and latitudinal gradient, $\Omega_{,\theta}$, of the solar rotation rate obtained using GONG and MDI data. Panels in the upper row show the cuts at fixed latitude as a function of radius, while those in the lower row shows the same results as color-coded diagrams. All values are in units of $\text{nHz } R_{\odot}^{-1}$.

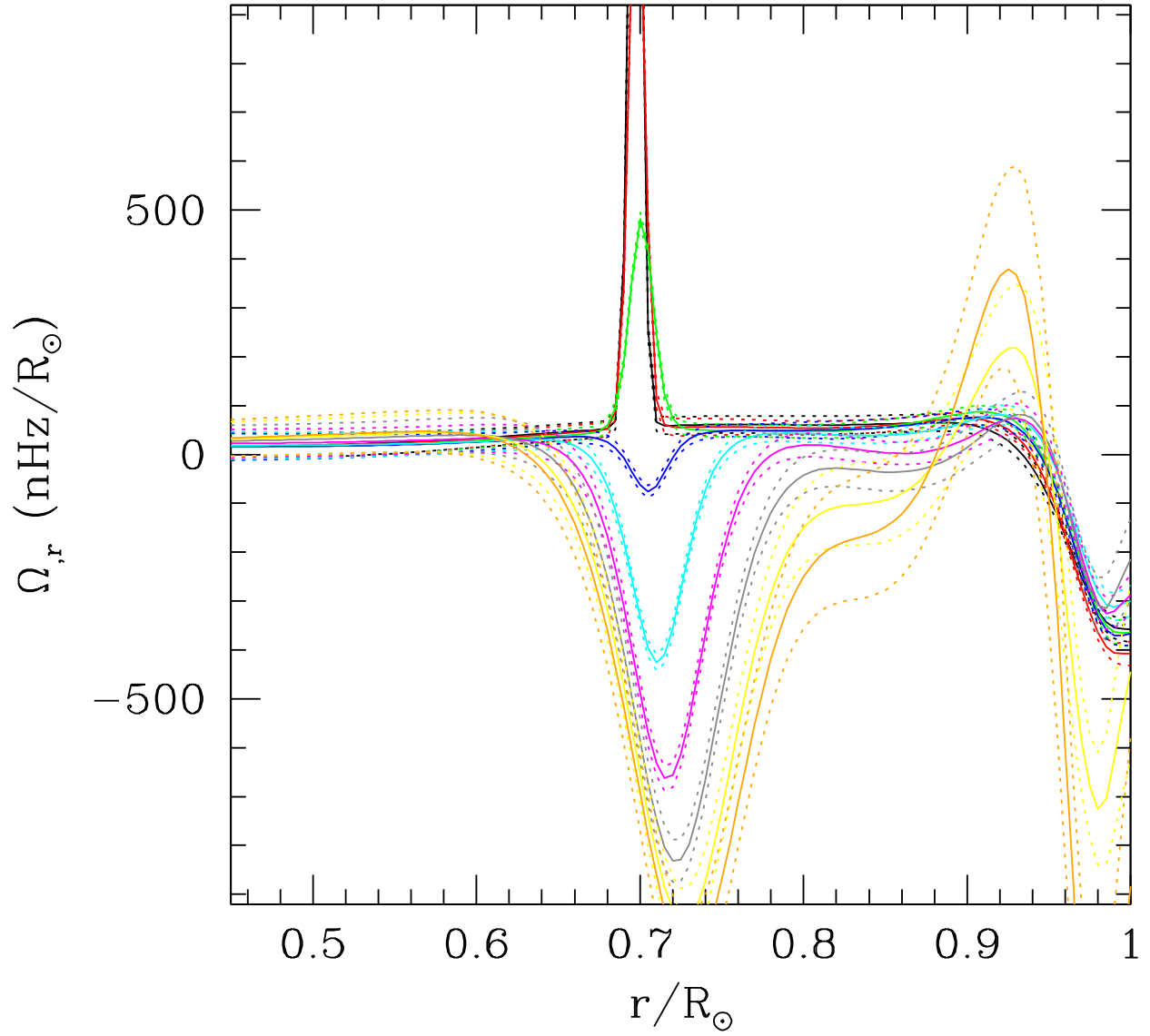


Fig. 2.— The mean radial gradient, $\Omega_{,r}$, obtained from MDI data using the tachocline model of Antia et al. (1998) shown at a few selected latitudes. The color scheme is same as that in the upper row of Fig. 1. Errorbars are shown by dotted lines.

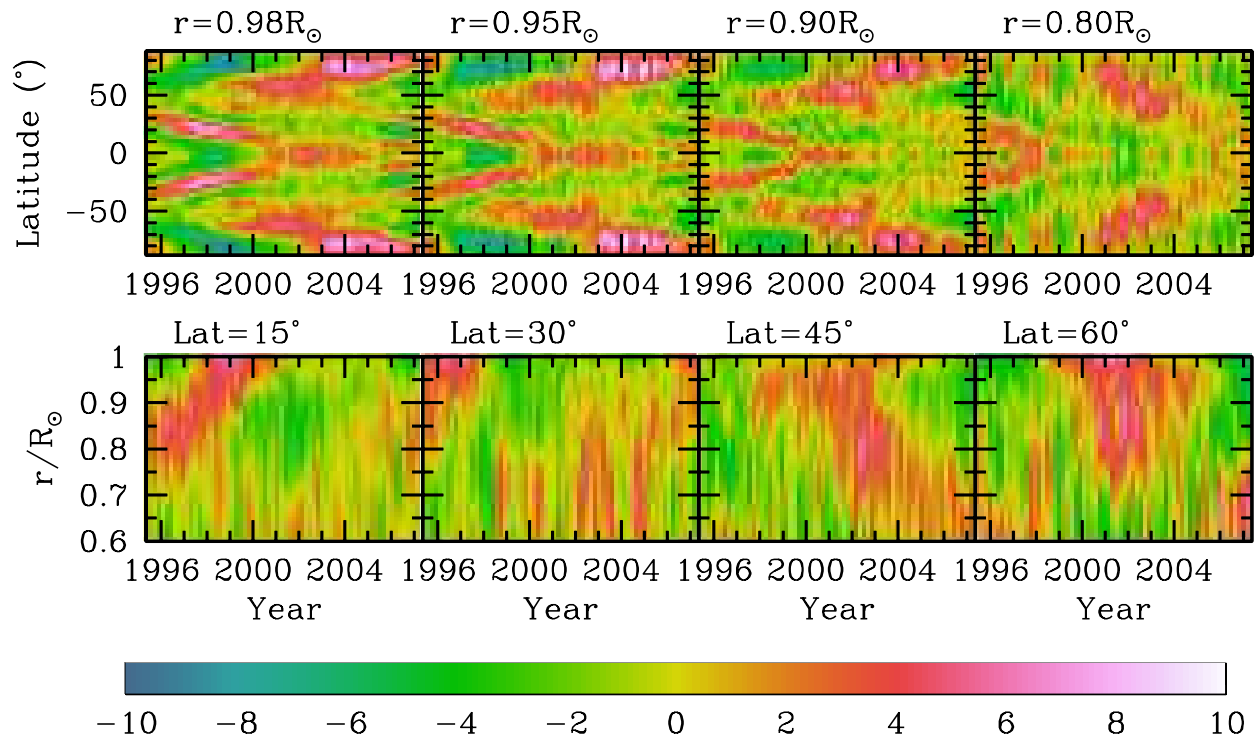


Fig. 3.— Diagrams showing δv_ϕ , the residuals of the rotation velocity obtained using GONG data. We show the results at a few representative depths and latitudes as marked above the respective panels. The scale is in m s^{-1} .

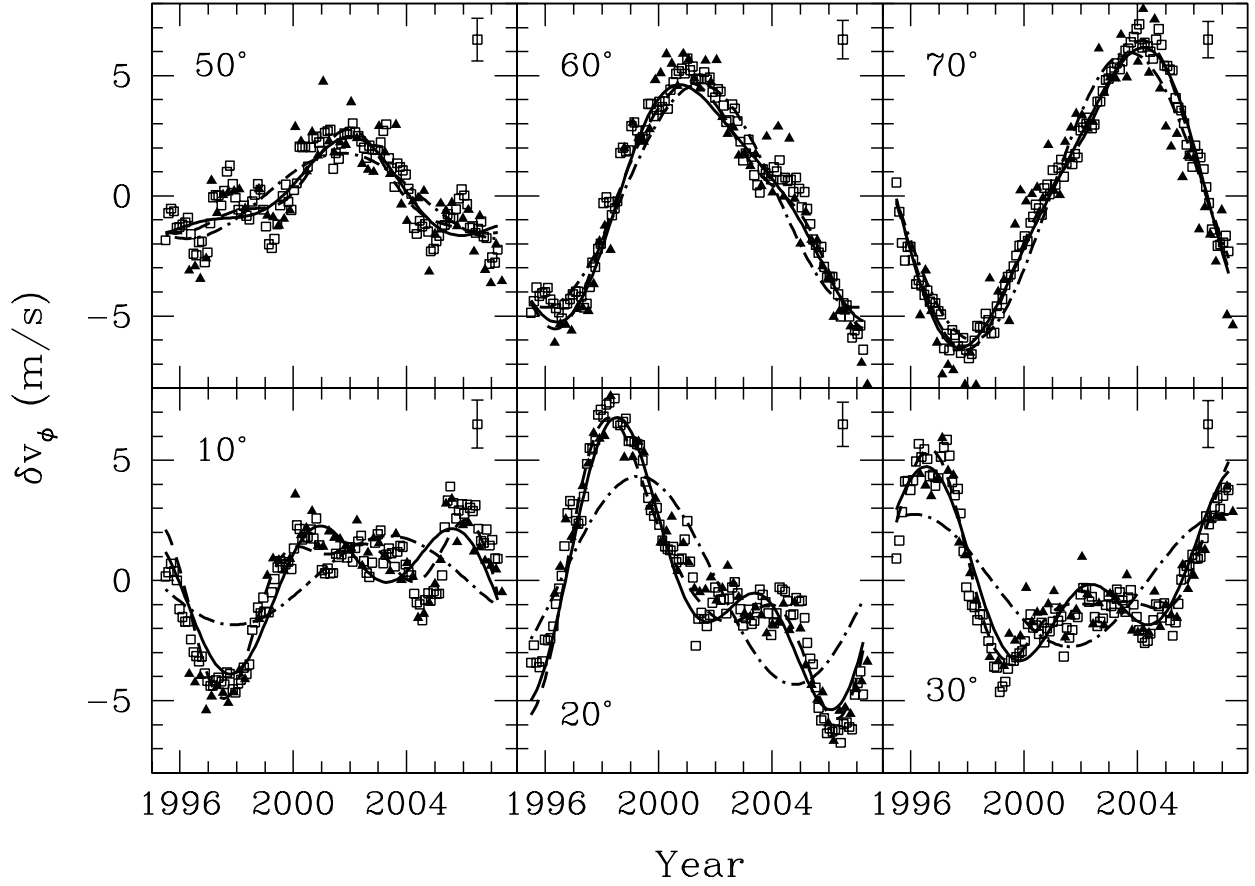


Fig. 4.— The zonal-flow velocity as a function of time at different latitudes at $r = 0.98R_\odot$. The latitudes are marked in each panel. The squares show results obtained with GONG data, while triangles show results with MDI data. The dash-dotted, solid and dashed lines show the fits using Eq. (2) to the GONG results with 1,2 and 3 terms respectively. For clarity, errorbars are not shown on the points, however, a typical errorbar is shown by a point in the upper right corner of each panel.

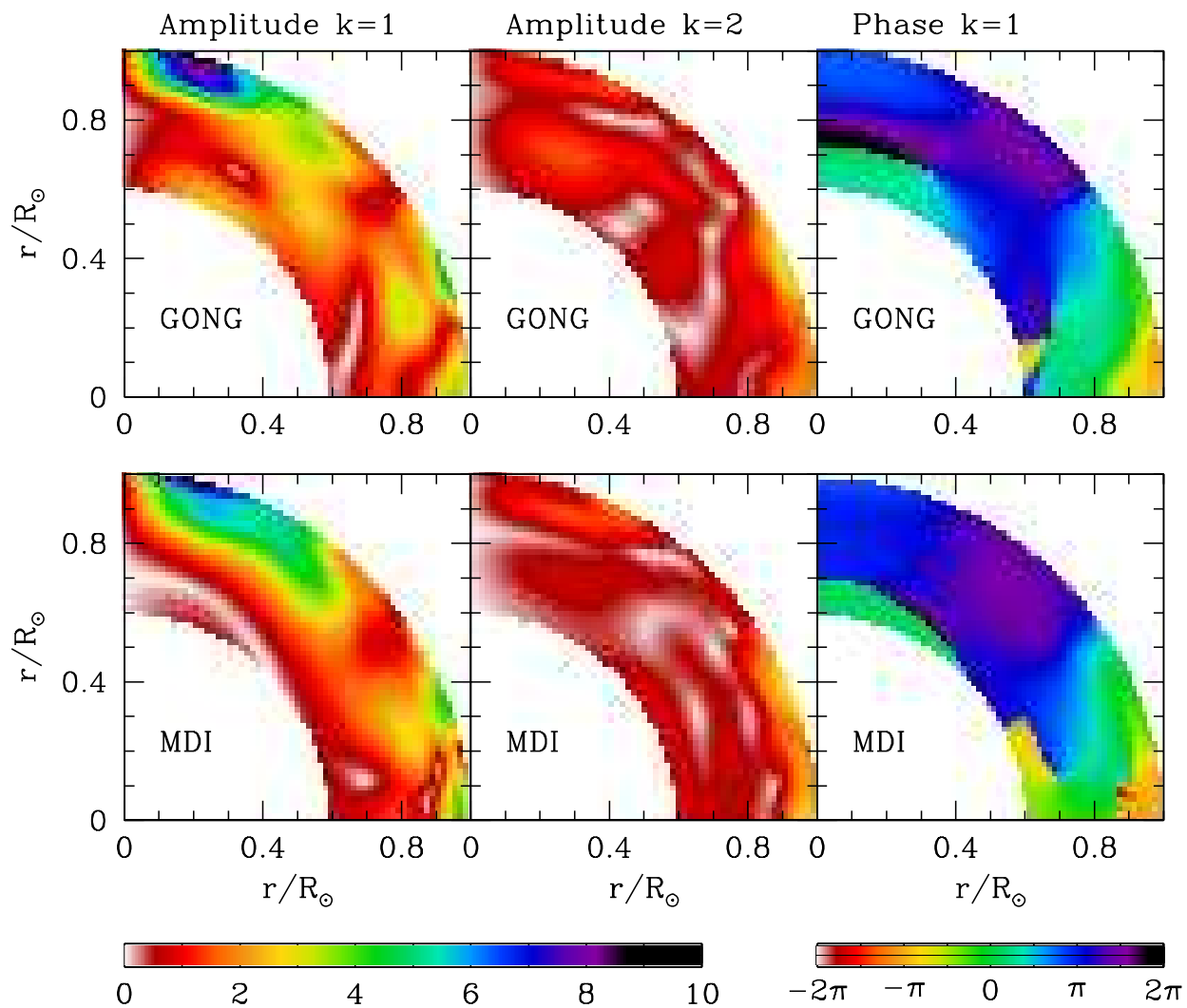


Fig. 5.— Diagram showing amplitudes of the $k = 1$ and $k = 2$ (Eq. 2) components and the phase of $k = 1$ component of zonal-flow expansion as obtained using GONG and MDI data. For panels that show the amplitudes, the scale is in units of m s^{-1} .

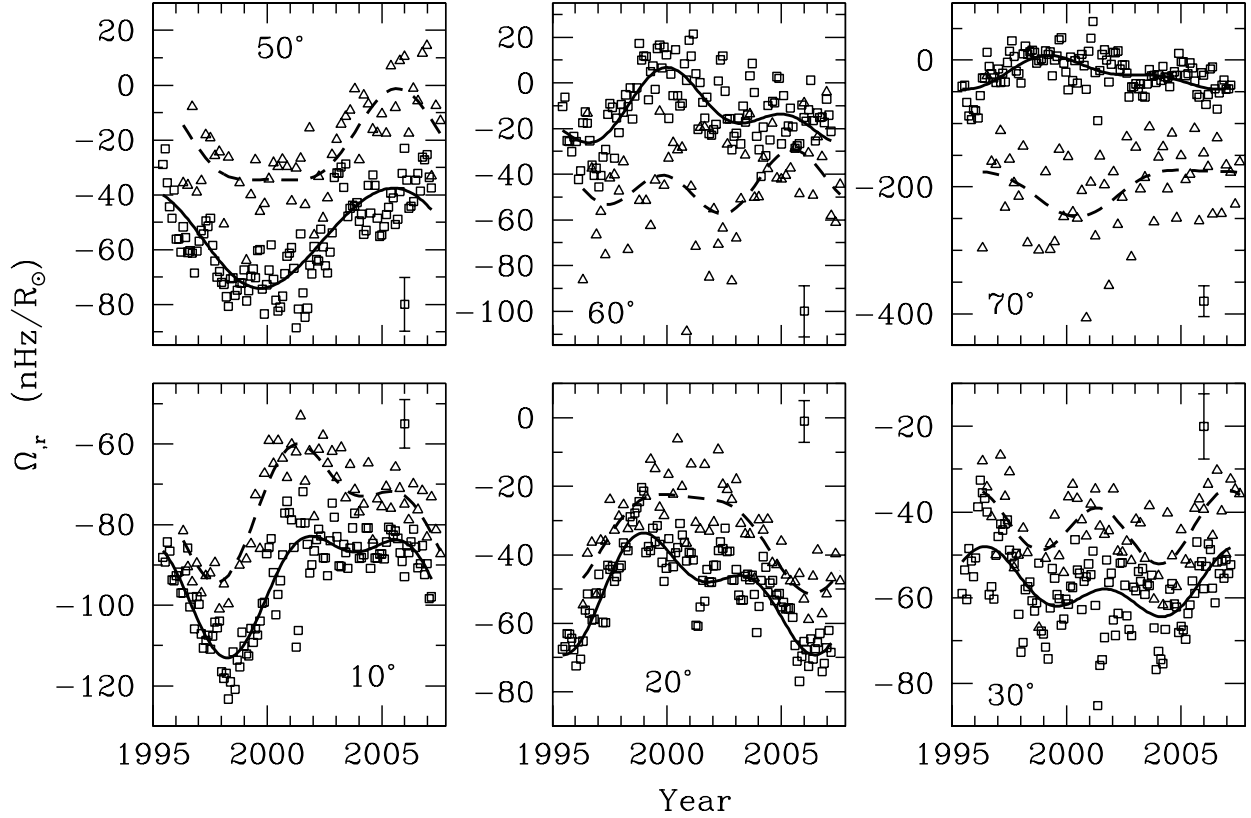


Fig. 6.— The radial gradient, Ω_r at a few selected latitudes is shown for $r = 0.95R_\odot$. The squares and triangles show results obtained using GONG and MDI data respectively. The solid and dashed lines show fits obtained using equations similar to Eq. (2) to these points. For clarity, errorbars are not shown on the points, but a typical errorbar is shown by a point in a corner of each panel.

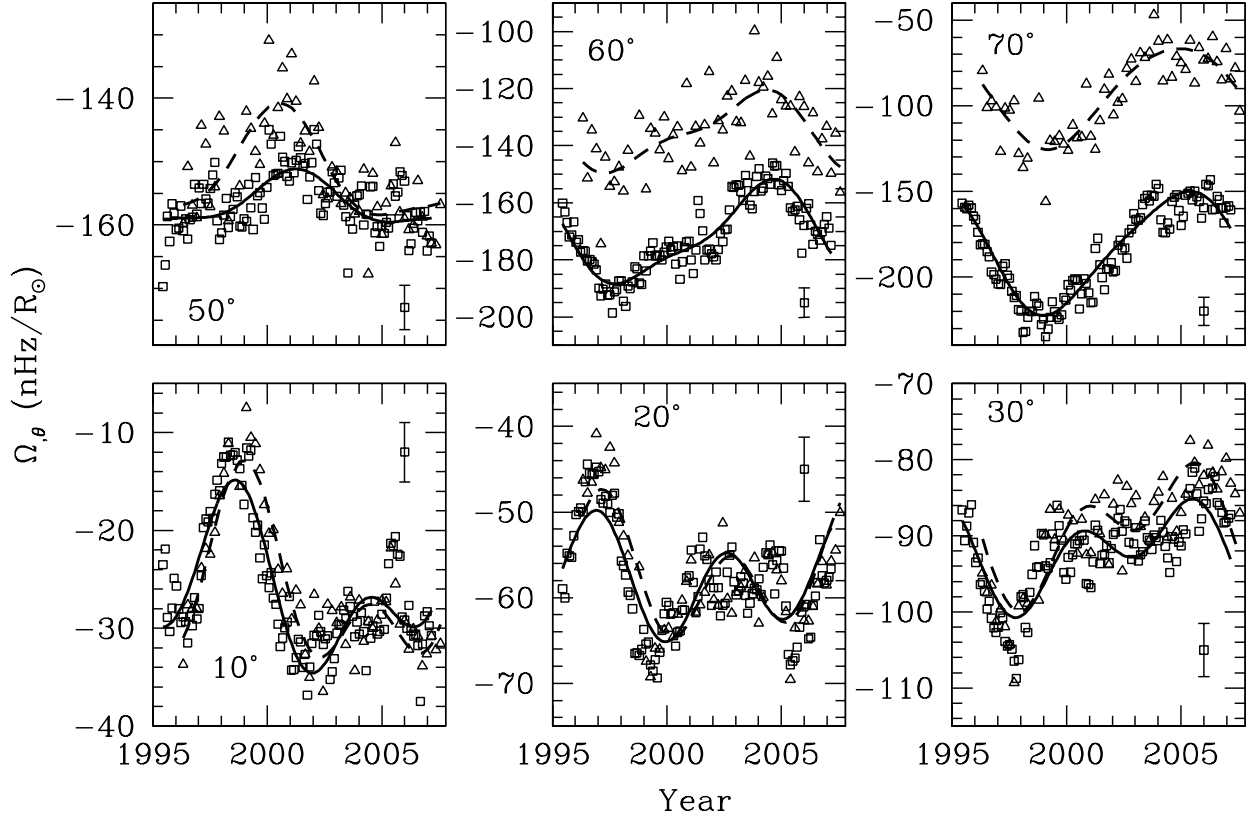


Fig. 7.— The latitudinal gradient Ω_θ at a few selected latitudes is shown for $r = 0.95R_\odot$. The squares and triangles show the results obtained using GONG and MDI data respectively. The solid and dashed lines show fits obtained using equations similar to Eq. (2) to these points. For clarity, errorbars are not shown on the points, but a typical errorbar is shown by a point in a corner of each panel.

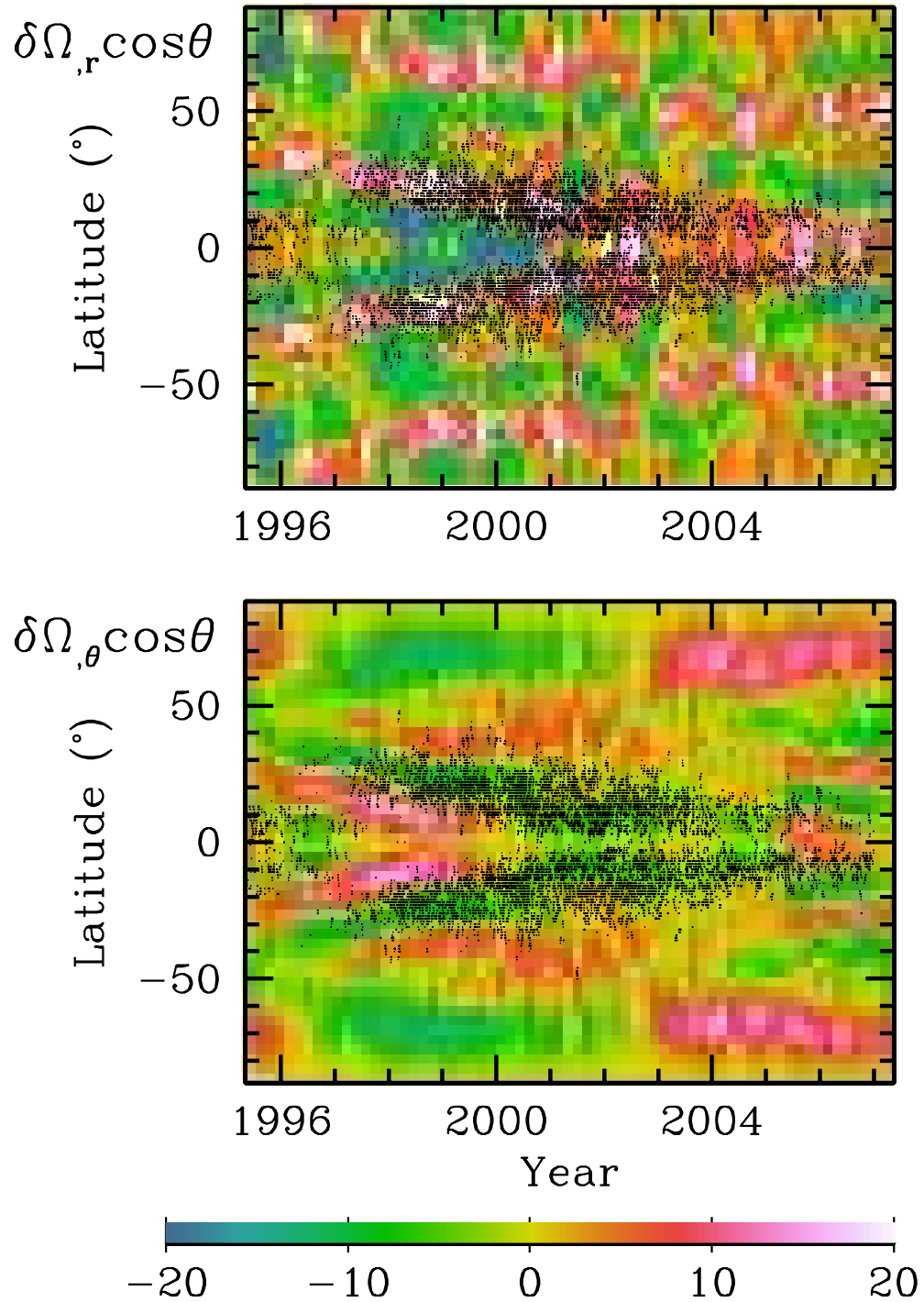


Fig. 8.— The radial and latitudinal gradients, at $r = 0.95R_{\odot}$ are superposed on the butterfly diagram showing the distribution of sunspots which is obtained from the Greenwich sunspot data. The scale is marked in $\text{nHz } R_{\odot}^{-1}$.

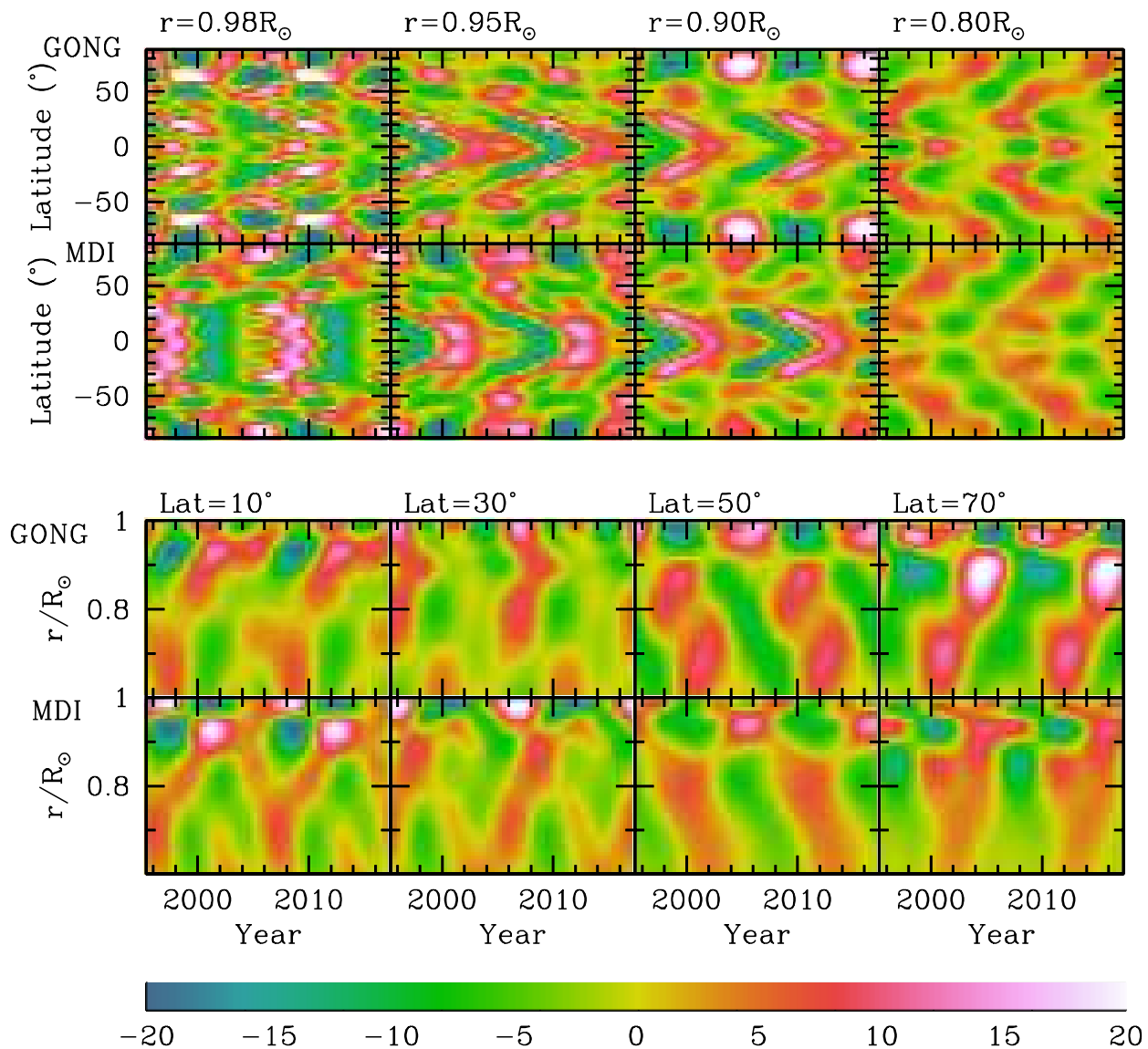


Fig. 9.— Residuals in the radial gradient obtained using GONG and MDI data at a few selected depths or latitudes. are shown. We actually show $\delta\Omega_r \cos\theta$ to minimize latitudinal variation. The scale is marked in units of $\text{nHz } R_{\odot}^{-1}$.

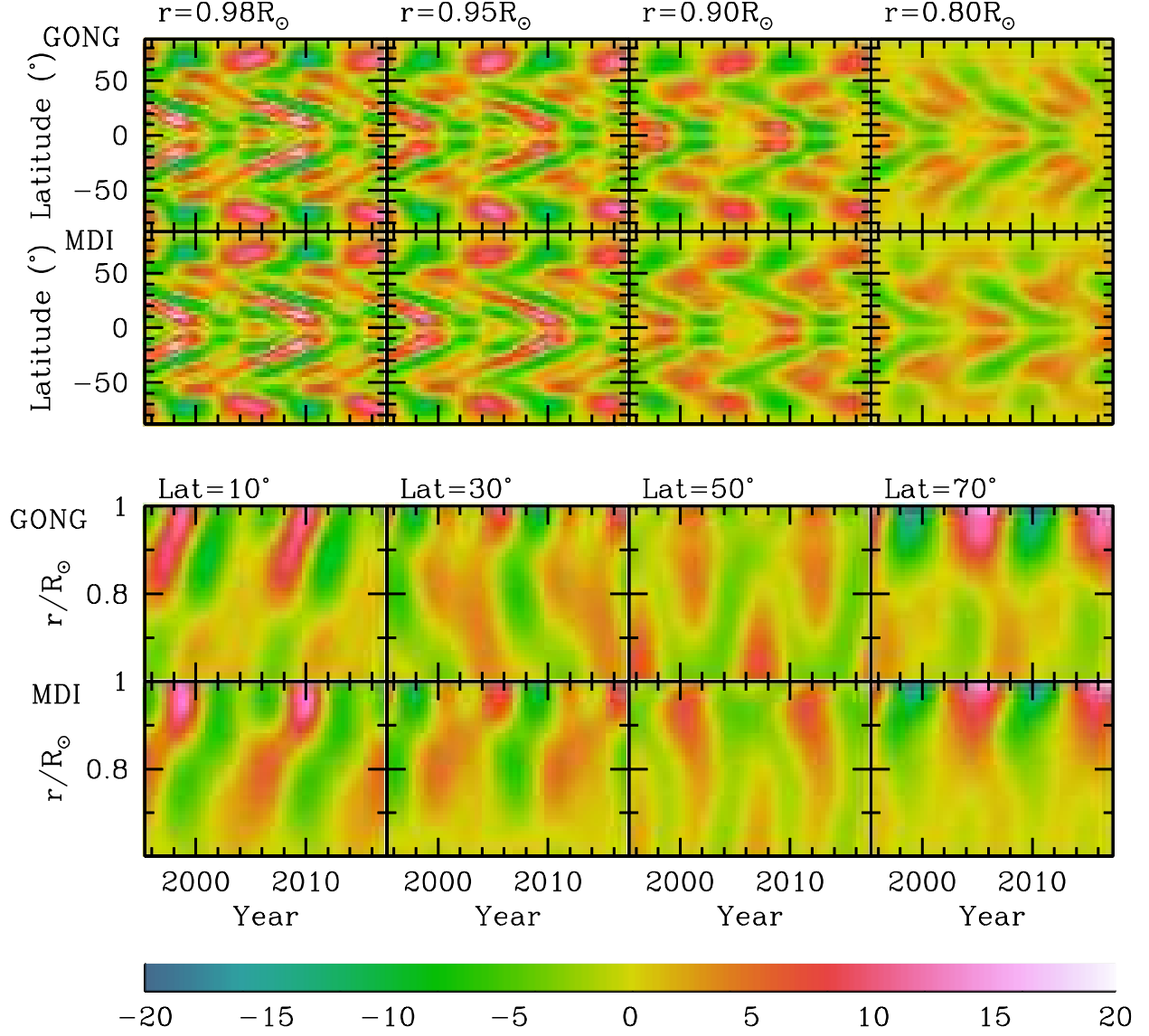


Fig. 10.— Residual in the latitudinal gradient obtained using GONG and MDI data at a few selected depths or latitudes. We actually plot $\delta\Omega_{,\theta} \cos\theta$ to minimize latitudinal variation. The scale is marked in units of $\text{nHz } R_{\odot}^{-1}$.

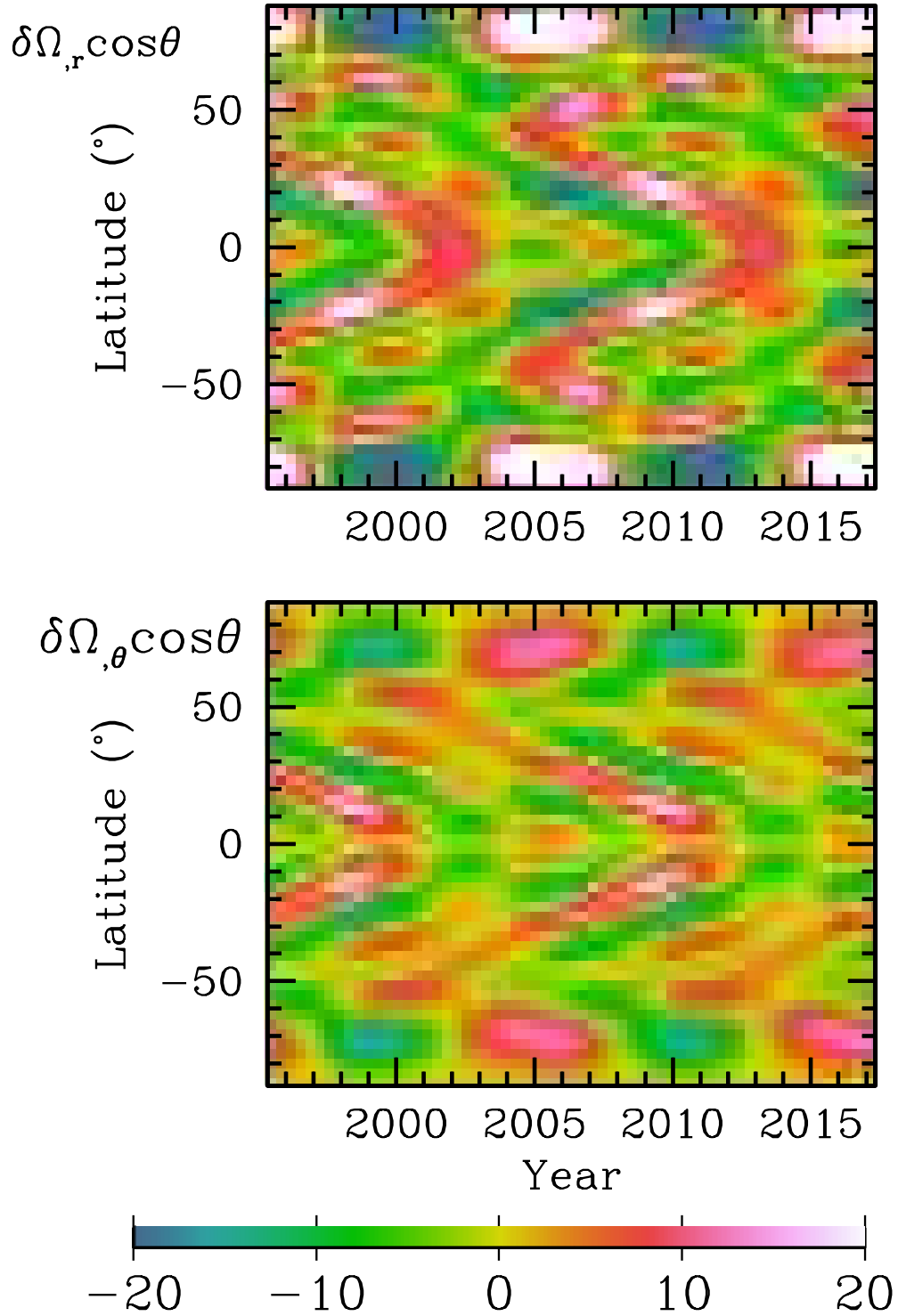


Fig. 11.— Residual in the radial and latitudinal gradient obtained at $r = 0.98R_\odot$ using MDI data with $\ell < 120$ modes. We actually plot $\delta\Omega_r \cos\theta$ and $\delta\Omega_\theta \cos\theta$ to minimize latitudinal variation. The scale is marked in units of $\text{nHz } R_\odot^{-1}$.

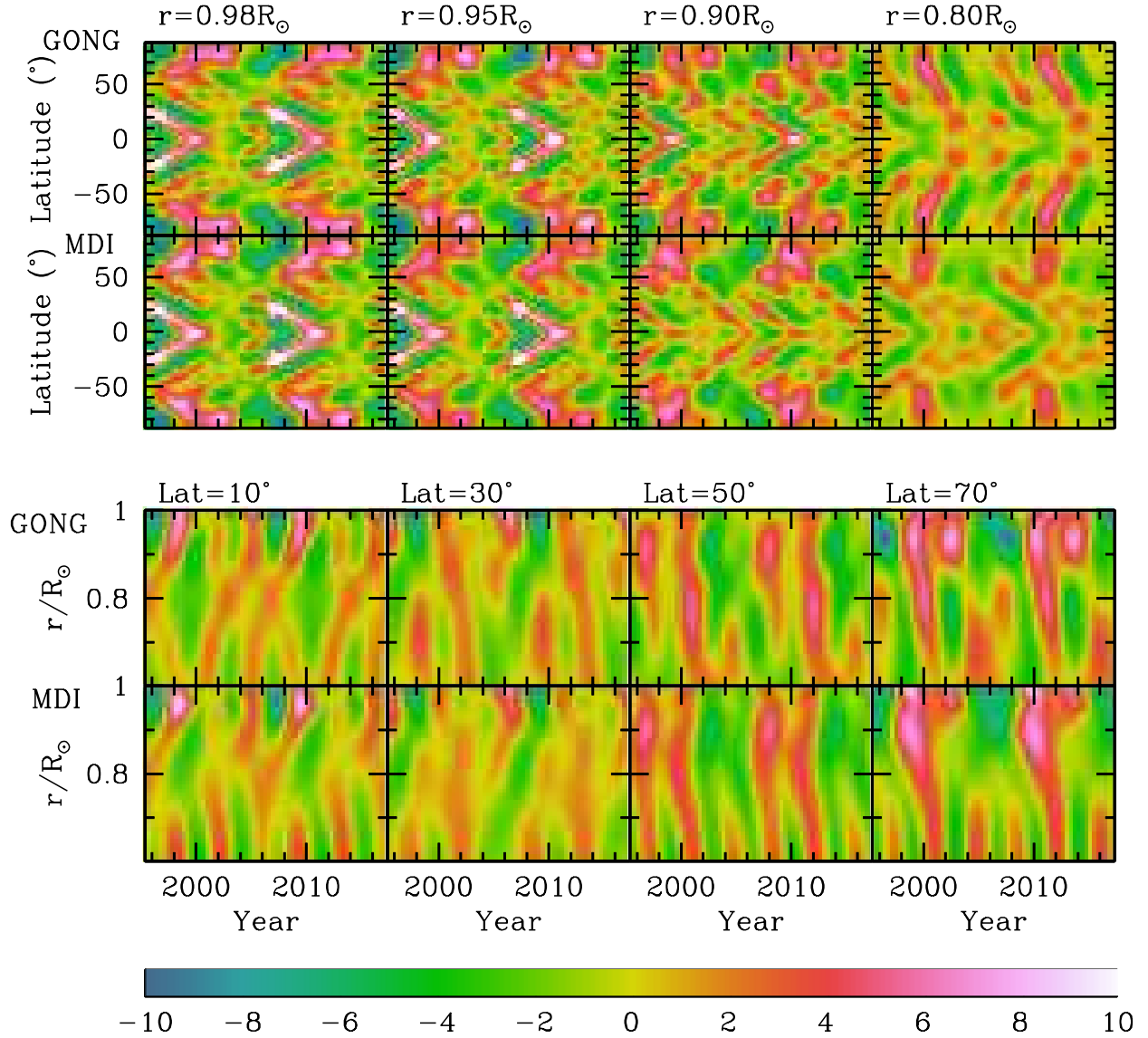


Fig. 12.— The acceleration $(1/\omega_0)\partial v_{\phi}/\partial t$ obtained using GONG and MDI data at a few selected depths or latitudes. The scale is marked in units of m s^{-1} .